On the Attenuation of the Perfectly Matched Layer in Electromagnetic Scattering Problems with the Spectral Element Method

I. Mahariq [1,3], M. Kuzuoğlu [2], and I. H. Tarman [3]

[1] Department of Electrical and Electronics Engineering
TOBB University of Economics and Technology, Ankara 06560, Turkey
ibmahariq@gmail.com

[2] Department of Electrical and Electronics Engineering
[3] Department of Engineering Sciences
Middle East Technical University, Ankara 06531, Turkey
kuzuoglu@metu.edu.tr, tarman@metu.edu.tr

Abstract ─ Although Spectral Element Method (SEM) has been applied in the modeling of boundary value problems of electromagnetics, its usage is not as common as the Finite Element or Finite Difference approaches in this area. It is well-known that the Perfectly Matched Layer (PML) approach is a mesh/grid truncation method in scattering or radiation applications where the spatial domain is unbounded. In this paper, the PML approach in the SEM context is investigated in two-dimensional, frequency-domain scattering problems. The main aim of this paper is to provide the PML parameters for obtaining an optimum amount of attenuation in the scattered field per wavelength in the PML region for Legendre-Gauss-Lobatto grids. This approach is extended to the analysis of SEM accuracy in scattering by electrically large objects by taking the free space Green's function as the building block of the scattered field. Numerical results presented in this work demonstrate the ability of achieving a high degree of accuracy of SEM as compared to other finite methods, as well as the successful applicability of the PML in electromagnetic scattering problems in terms of the optimum attenuation factors provided in this work.

Index Terms ─ Attenuation, electromagnetic scattering, Green's function, Legendre polynomials, perfectly matched layer, spectral element method.

I. INTRODUCTION

The well-known Perfectly Matched Layer (PML) approach, (with its possible realizations; the split-field formulation [1], the anisotropic realization [2], and the bianisotropic realization [3]), showed superiority over Absorbing Boundary Conditions (ABCs) when imposed to truncate computational domains in the numerical modeling of electromagnetic radiation and/or scattering problems [4]. The most commonly used numerical methods, namely Finite Element Method (FEM) and Finite Difference Method (FDM), have been extensively applied and investigated in electromagnetic scattering problems where PML is utilized for mesh truncation. Spectral Element Method (SEM) on the other hand, has not been used in this field as much as finite element or finite difference methods.

SEM can be considered as a generalization of FEM with special choice of nodal points and quadrature integration points. It is the high degree of accuracy, the lower CPU time and memory requirement, when compared with other numerical methods, that makes it worthy to use SEM in electromagnetic scattering [5,6,7,8]. These attractive features of SEM are the outcomes of introducing higher degree basis functions that results in having the minimal number of

Submitted On: March 1, 2014
Accepted On: September 6, 2014

unknowns; and consequently, the computational cost is much reduced at the same accuracy.

The main goal of this paper is the investigation of the optimal choice of the PML attenuation factor in two-dimensional scattering problems governed by Helmholtz equation. This formulation yields a mathematical model for electromagnetic (transverse electric or magnetic) and acoustic scattering problems. In FEM or FDM approaches, the PML may include several elements/grid points. In this case, the choice of the attenuation factor depends on the thickness of the PML, as well as the density of the nodes/grid points in the layer. Numerical experiments have demonstrated that the PML thickness must be about one wavelength, and the number of nodes/grid points in the longitudinal direction must be 15 to 20 to represent the exponential decay adequately. In the context of SEM, no such analysis has been carried out in the literature. The interest for such an analysis arises from two facts; first, the distribution of grid points in SEM is standard (consider Legendre-Gauss-Lobatto grids), while in FEM or FDM is not. The regularity in the elements corresponding to PML region is another important point. In this paper, the PML region is constructed as a single layer of SEM elements with dimensions equal to a wavelength. Under this restriction, the optimal choice of the attenuation factor is carried out via numerical experiments. Next, the chosen values of the attenuation factor are used to study the accuracy of SEM when applied in scattering problems by large objects.

The paper is arranged as follows: in Section II, the formulation of PML approach in 2D frequency domain scattering problems is presented. In Section III, the approximation of Helmholtz equation by SEM with PML, is given. Section IV demonstrates the numerical results, and finally some conclusions are presented in Section V.

II. PML FORMULATION IN 2D SCATTERING PROBLEMS

In the following, y axis (i.e.: x=0) is taken as the interface between Ω and Ω_{PML}, which stand for free space and PML regions, respectively, as depicted in Fig. 1. $\Omega=\{(x,y)|x<0\}$, $\Omega_{PML}=\{(x,y)|x>0\}$. A plane wave (with suppressed time dependence $\exp(j\omega t)$) incident to the interface can be expressed as:

$$u(x,y)=e^{-jk(\cos\theta x+\sin\theta y)}, \tag{1}$$

in which u(x,y) is the scalar field at the point (x,y), θ is the incident angle (angle between the direction of propagation of the plane wave and x-axis), and k is defined as:

$$k=\frac{2\pi}{\lambda}, \tag{2}$$

which is called the wave number, with λ being the wavelength. As pointed out in [4], in order to provide the attenuation required in domain truncation, one needs to multiply the wave in the PML region by a function f(x) satisfying two properties: f(0)=1, and f(x) decreases monotonically for x>0. For instance, f(x) can be chosen as:

$$f(x)=e^{-\alpha\cos\theta x}. \tag{3}$$

The scalar field in Ω_{PML} then takes the form:

$$u(x,y)=e^{-jk(a\cos\theta x+\sin\theta y)}, \tag{4}$$

where

$$a=1+\frac{\alpha}{jk}, \tag{5}$$

and α is a positive real constant (called the attenuation factor). By direct differentiation, we obtain the following partial differential equation satisfied by the field:

$$\frac{1}{a^2}\frac{\partial^2 u}{\partial x^2}+\frac{\partial^2 u}{\partial y^2}+k^2u=0. \tag{6}$$

It is obvious that from the first property of f(x), the continuity condition at the interface holds:

$$u\big|_{-0}=u\big|_{+0}. \tag{7}$$

The second condition can be directly derived from (1) and (4) as:

$$\left.\frac{\partial u}{\partial x}\right|_{-0}=\frac{1}{a}\left.\frac{\partial u}{\partial x}\right|_{+0}. \tag{8}$$

While applying integration by parts, the second condition is automatically satisfied if Helmholtz equation in PML region is rewritten as:

$$\frac{1}{a}\frac{\partial^2 u}{\partial x^2}+a\frac{\partial^2 u}{\partial y^2}+a\,k^2u=0. \tag{9}$$

It can easily be shown that for a horizontal interface (i.e.: y=0) the following equation is obtained (while keeping PML thickness the same; i.e., the same attenuation factor, α):

$$\frac{\partial^2 u}{\partial x^2}+\frac{1}{a^2}\frac{\partial^2 u}{\partial y^2}+k^2u=0. \tag{10}$$

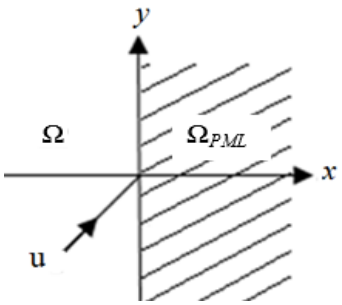

Fig. 1. The interface between Ω and Ω_{PML}.

And finally for a corner region, which is the intersection of vertical and horizontal PML regions, the attenuation is applied in both directions [4], and the following partial differential equation is obtained (see Fig. 2):

$$\frac{1}{a^2}\frac{\partial^2 u}{\partial x^2}+\frac{1}{a^2}\frac{\partial^2 u}{\partial y^2}+k^2u=0, \qquad (11)$$

or:

$$\frac{\partial^2 u}{\partial x^2}+\frac{\partial^2 u}{\partial y^2}+a^2k^2u=0. \qquad (12)$$

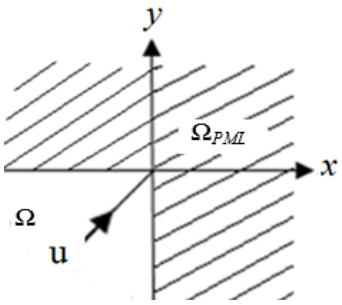

Fig. 2. The corner interface between Ω and Ω_{PML}.

Ideally, the attenuation factor (α) must be infinitely large to make sure that the field magnitude is immediately forced to zero in the PML region. However, in numerical applications, the PML must be terminated by an outer boundary and one must search for the optimum PML thickness, discretization (i.e.: mesh/grid density especially in the longitudinal direction), and α, in order to represent the field decay as smoothly as possible without causing "numerical" reflections. In other words, there is a tradeoff in the choice of the attenuation factor in having almost zero Dirichlet boundary condition on the outer PML boundary and providing the adequate rate of attenuation within PML for a specific mesh/grid.

III. SEM FORMULATION OF HELMHOLTZ EQUATION

In scattering problems governed by Helmholtz equation, Sommerfeld radiation condition is satisfied:

$$\lim_{|r|\to\infty}\sqrt{|r|}\left(\frac{\partial u}{\partial n}-jku\right)=0, \qquad (13)$$

where r is the radiation direction. However, it is hard to apply this condition in SEM. Therefore, we use PML to truncate the computational domain. Based on the PML formulation given in Section II, and as seen from Fig. 4, the problem is defined as:

$$\nabla\Lambda\nabla u+ak^2u=0, \qquad (14a)$$

for $\mathbf{x}=(x,y)\in\Omega\subset\Re^2$ subject to the boundary conditions:

$$u\big|_{\partial\Omega_D}=f,\quad \tfrac{\partial}{\partial n}u\big|_{\partial\Omega_N}=g, \qquad (14b)$$

on the boundary $\partial\Omega=\partial\Omega_D\bigcup\partial\Omega_N$. Λ is a tensor defined as:

$$\Lambda=\begin{bmatrix}\Lambda_{11} & 0\\ 0 & \Lambda_{22}\end{bmatrix}, \qquad (14c)$$

where

$$\begin{bmatrix}\Lambda_{11} & \Lambda_{22}\end{bmatrix}=\begin{bmatrix}\frac{1}{a} & a\end{bmatrix}\text{ for x-decay,}$$

$$\begin{bmatrix}\Lambda_{11} & \Lambda_{22}\end{bmatrix}=\begin{bmatrix}a & \frac{1}{a}\end{bmatrix}\text{ for y-decay,}$$

$$\begin{bmatrix}\Lambda_{11} & \Lambda_{22}\end{bmatrix}=\begin{bmatrix}\frac{1}{a} & \frac{1}{a}\end{bmatrix}\text{ for a corner region,}$$

and $a=1$ for Ω_{FS}.

SEM formulation involves two function spaces, namely, test and trial spaces. An approximate solution to (14) is sought in the trial space:

$$U=\left\{u\in H\,|\,u\big|_{\partial\Omega_D}=f,\quad \tfrac{\partial}{\partial n}u\big|_{\partial\Omega_N}=g\right\}. \qquad (15)$$

The residual resulting from the substitution of the approximate solution from the trial space into (14) vanishes in the process of projection onto the test space:

$$V=\{v\in H\,|\,v\big|_{\partial\Omega_D}=0\}. \qquad (16)$$

The projection is performed by using the weighted inner product operation:

$$\left(\mathrm{v},\mathrm{u}\right)_{\omega} \equiv \int_{\Omega} \omega\,\bar{\mathrm{v}}\,\mathrm{u}\,\mathrm{d}\mathbf{x}, \tag{17}$$

in the Hilbert space H where overbar denotes complex conjugation. The projection procedure:

$$(\mathrm{v}, \nabla\Lambda\nabla\,\mathrm{u} + \mathrm{a}\,\mathrm{k}^2\mathrm{u})_{\omega} = 0, \tag{18}$$

leads to the variational (weak) form:

$$\int_{\Omega} \nabla(\omega\bar{\mathrm{v}})\,\Lambda\nabla\,\mathrm{u}\,\mathrm{dx} - \mathrm{a}\,\mathrm{k}^2 \int_{\Omega} \omega\bar{\mathrm{v}}\,\mathrm{u}\,\mathrm{dx} = \int_{\partial\Omega_N} \omega\bar{\mathrm{v}}\,\mathrm{g}\,\mathrm{dx}, \tag{19}$$

after integration by parts that introduces the boundary integrals. The trial function is then decomposed as follows:

$$\mathrm{u} = \mathrm{u_h} + \mathrm{u_b} \text{ where } \mathrm{u_h}\big|_{\partial\Omega_D} = 0, \text{ and } \mathrm{u_b}\big|_{\partial\Omega_D} = \mathrm{f}, \tag{20}$$

resulting in:

$$\int_{\Omega} \nabla(\omega\bar{\mathrm{v}})\,\Lambda\nabla\,\mathrm{u_h}\,\mathrm{d}\mathbf{x} - \mathrm{ak}^2 \int_{\Omega} \omega\bar{\mathrm{v}}\,\mathrm{u_h}\,\mathrm{dx} = -$$

$$\int_{\Omega} \nabla(\omega\bar{v})\,\Lambda\nabla\,\mathrm{u_b}\,\mathrm{dx} + \mathrm{ak}^2 \int_{\Omega} \omega\bar{\mathrm{v}}\,\mathrm{u_b}\,\mathrm{dx} \int_{\partial\Omega_N} \omega\bar{\mathrm{v}}\,\mathrm{g}\,\mathrm{dx}, \tag{21}$$

after substitution into (19). The boundary conditions are now in place in the variational form with the introduction of the particular solution $\mathrm{u_b}$ satisfying the nonhomogeneous Dirichlet boundary condition. Adapting the formulation to arbitrary domain geometry is achieved in two steps. The first step involves partitioning of the domain into mutually disjoint elements:

$$\Omega = \Omega^1 \cup \ldots \cup \Omega^{\mathrm{e}} \ldots \cup \Omega^{\mathrm{M}} = \bigcup_{\mathrm{e}=1}^{\mathrm{M}} \Omega^{\mathrm{e}}. \tag{22}$$

A typical integral in the variational form then becomes:

$$\int_{\Omega} \omega\bar{\mathrm{v}}\,\mathrm{u_h}\,\mathrm{d}\mathbf{x} = \sum_{\mathrm{e}=1}^{\mathrm{M}} \int_{\Omega^{\mathrm{e}}} \omega\bar{\mathrm{v}}\,\mathrm{u_h}\,\mathrm{d}\mathbf{x}, \tag{23}$$

due to the linearity of integration operation. The second step is the introduction of the standard square element:

$$\Omega^{\mathrm{std}} = \left\{(\xi,\eta) \in \Re^2 \mid -1 \le \xi \le 1, -1 \le \eta \le 1\right\}, \tag{24}$$

that will standardize and facilitate the integral operations over a general quadrilateral element Ω^{e} with curved sides through mapping:

$$\mathrm{x} = \chi_1^{\mathrm{e}}(\xi,\eta), \quad \mathrm{y} = \chi_2^{\mathrm{e}}(\xi,\eta). \tag{25}$$

The operations can then be converted using the rules:

$$\begin{bmatrix} \mathrm{dx} \\ \mathrm{dy} \end{bmatrix} = \underbrace{\begin{bmatrix} \frac{\partial\chi_1^{\mathrm{e}}}{\partial\xi} & \frac{\partial\chi_1^{\mathrm{e}}}{\partial\eta} \\ \frac{\partial\chi_2^{\mathrm{e}}}{\partial\xi} & \frac{\partial\chi_2^{\mathrm{e}}}{\partial\eta} \end{bmatrix}}_{\mathbf{J}} \begin{bmatrix} \mathrm{d}\xi \\ \mathrm{d}\eta \end{bmatrix},$$

$$\nabla = \begin{bmatrix} \frac{\partial}{\partial\mathrm{x}} \\ \frac{\partial}{\partial\mathrm{y}} \end{bmatrix} = \frac{1}{|\mathbf{J}|} \begin{bmatrix} \frac{\partial\chi_2^{\mathrm{e}}}{\partial\eta} & -\frac{\partial\chi_1^{\mathrm{e}}}{\partial\eta} \\ -\frac{\partial\chi_2^{\mathrm{e}}}{\partial\xi} & \frac{\partial\chi_1^{\mathrm{e}}}{\partial\xi} \end{bmatrix} \begin{bmatrix} \frac{\partial}{\partial\xi} \\ \frac{\partial}{\partial\eta} \end{bmatrix}, \tag{26}$$

where $|\mathrm{J}|$ is the determinant of the Jacobian J.

Numerical implementation of the procedure requires introduction of a spatial discretization that will facilitate the numerical evaluation of the derivatives and the integrals. This is equivalent to taking the trial and test spaces as finite dimensional spaces for which space of polynomials is the convenient choice. Jacobi polynomials as eigenfunctions of singular Sturm-Liouville differential operator provide a good basis for this space [8]. Numerically stable interpolation and highly accurate quadrature integration approximation techniques are provided by nodes and weights associated with Jacobi polynomials. In particular, Legendre polynomials are the convenient choice in that they are orthogonal under the weighted inner product with unity weight $\omega = 1$. The associated roots ς_{m} as nodes provide the stable form of interpolation:

$$\mathrm{u}(\varsigma) = \sum_{\mathrm{m}=0}^{\mathrm{N}} \mathrm{u}(\varsigma_{\mathrm{m}})\mathrm{L}_{\mathrm{m}}(\varsigma), \tag{27}$$

where L denotes respective Lagrange interpolants with the typical form

$$\mathrm{L}_{\mathrm{k}}(\varsigma) = \prod_{\substack{\ell=0 \\ \ell\neq\mathrm{k}}}^{\mathrm{N}} \frac{(\varsigma-\varsigma_\ell)}{(\varsigma_{\mathrm{k}}-\varsigma_\ell)}, \tag{28}$$

satisfying the cardinality property $\mathrm{L}_{\mathrm{k}}(\varsigma_\ell) = \delta_{\mathrm{k}\ell}$. This in turn provides the means for evaluating the derivatives, say:

$$\frac{\mathrm{d}}{\mathrm{d}\varsigma}\mathrm{u}(\varsigma)\Big|_{\varsigma_{\mathrm{k}}} = \sum_{\mathrm{m}=0}^{\mathrm{N}} \mathrm{u}(\varsigma_{\mathrm{m}})\mathrm{L}'_{\mathrm{m}}(\varsigma_{\mathrm{k}}) = \sum_{\mathrm{m}=0}^{\mathrm{N}} \mathrm{u}(\varsigma_{\mathrm{m}}) \underbrace{\mathrm{L}'_{\mathrm{m}}(\varsigma_{\mathrm{k}})}_{\mathrm{D_{km}}}, \tag{29}$$

where $\mathrm{D_{km}}$ is referred to as the differentiation matrix. It also provides Gauss-Legendre-Lobatto (GLL) quadrature:

$$\int_{-1}^{1} \mathrm{u}(\varsigma)\,\mathrm{d}\varsigma = \sum_{\mathrm{k}=0}^{\mathrm{N}} \varpi_{\mathrm{k}}\mathrm{u}(\varsigma_{\mathrm{k}}), \tag{30}$$

which is exact for the integrand a polynomial of degree $\leq 2N-1$. These can easily be extended to two dimensions over the tensor grid (ξ_k, η_ℓ) with the mapping functions $\chi_i(\xi,\eta)$ constructed using the linear blending function approach [9,10].

IV. NUMERICAL RESULTS

A. Optimum attenuation factor

For the numerical experiments, it is assumed that u is known (analytical expression is available). In Fig. 3, on $\partial\Omega_1$ and $\partial\Omega_2$, u is imposed as a Dirichlet boundary condition (this is referred as "Case-a"). In Ω, u satisfies the homogenous Helmholtz equation. The numerical solution by SEM is then found. In Fig. 4, where the computational domain $\Omega = \Omega_{FS} \bigcup \Omega_{PML}$, u is imposed on $\partial\Omega_1$ only, and on $\partial\Omega_2$ zero Dirichlet boundary condition is simply imposed. This case is referred as "Case-b", in which both the homogenous Helmholtz equation (governing the free space region, Ω_{FS}), and the PML partial differential equations (governing the PML region, Ω_{PML}) are satisfied. In this way, the SEM error without the PML (Case-a) and the SEM error with the utilization of the PML can be observed.

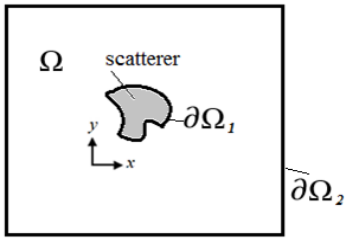

Fig. 3. The computational domain definition without the PML.

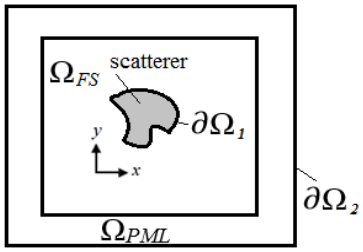

Fig. 4. The computational domain definition with the PML.

For sake of determining the optimum value of α in SEM at a fixed number of points per wavelength in PML region, several problems have been carefully studied. First, we considered the two-dimensional Green's function that has Helmholtz equation as the governing PDE:

$$\nabla^2 u + k^2 u = -\delta(\vec{r}), \qquad (31)$$

where the solution is given in terms of Hankel function of the second kind of order zero as $u(\vec{r}) = (j/4)\,H_0^{(2)}(k|\vec{r}|)$. To avoid singularity arising from the radiating point source being at the origin, we truncate the domain around the origin, and impose the Dirichlet boundary condition in terms of the field $u(\vec{r})$ over the boundary $\partial\Omega_1$ as shown in Fig. 5 (a). Then, to have a bounded domain, truncation by PML is applied. By utilizing the symmetry, only one-fourth of the computational domain is studied. Zero Dirichlet boundary is imposed on outer boundary of the PML region (i.e.: $\partial\Omega_2$) and zero Neumann symmetry condition is imposed on the boundary $\partial\Omega_N$. The computational domain is subdivided into eight elements as shown in Fig. 5 (b), with dimensions of $\lambda \times \lambda$ and resolution of N×N for each element. It is worth to point that the maximum incident angle (the angle between the ray and the normal to the free space-PML interface) in this problem is 45° in terms of a ray approximation.

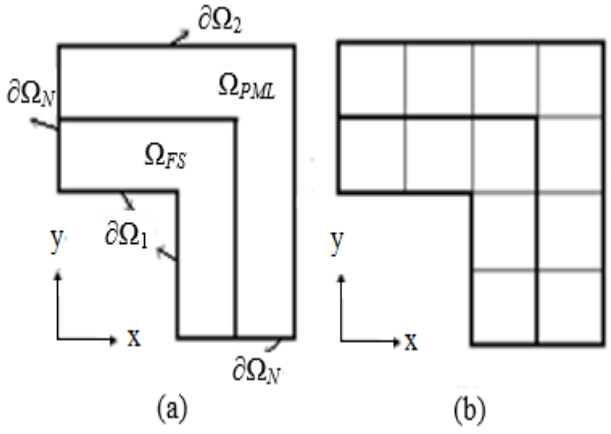

Fig. 5. The problem of the 2D Green's function: (a) the problem definition, and (b) elements in SEM.

Throughout of this paper, the error measure is defined as:

$$\mathrm{Err} = \max_{i} \frac{\left|u_{i,\mathrm{exact}} - u_{i,\mathrm{SEM}}\right|}{\left|u_{i,\mathrm{exact}}\right|}, \qquad (32)$$

where $u_{i,\mathrm{exact}}$ and $u_{i,\mathrm{SEM}}$ are the exact solution and the SEM solution, respectively, at the i^{th} node corresponding to the free space region, Ω_{FS}.

Table 1 shows the value of the attenuation factor (α), and the corresponding maximum relative error for each resolution (N). The values of α were well calibrated for each number of points per wavelength (N), such that the minimum possible error is obtained in each case. For instance, at N=11, the variation of against vs. α is presented in Fig. 6.

Table 1: Maximum relative errors obtained by SEM for the problem in Fig. 5

N	α	Err
7	4.40	4.5e-3
8	5.25	4.1746e-4
9	6.40	4.6100e-5
10	7.18	4.6486e-06
11	8.41	5.8466e-07
12	9.10	8.0365e-08
13	10.40	7.9952e-09
14	11.16	1.4402e-09
15	12.33	1.3769e-10
16	13.18	2.6012e-11
17	14.22	3.2078e-12
18	15.20	4.4765e-13

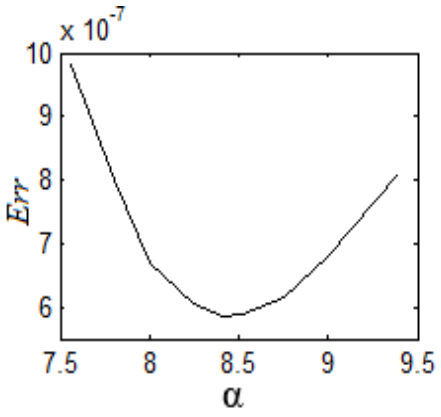

Fig. 6. Variation of SEM error vs. α at N=11.

It is important to check the accuracy of SEM when it is used to solve the 2D Green's function problem again, but this time, on a different computational domain in which the inner boundary is defined to be circular. Because of symmetry (i.e.: when the point source is placed at the origin), only two adjacent quadrants are studied as shown in Fig. 7 (a). Here, the field $u(\vec{r})$ is imposed over the inner boundary $\partial\Omega_1$, zero Dirichlet boundary condition and Neumann boundary condition are imposed on $\partial\Omega_2$ and $\partial\Omega_N$, respectively (Case-b). The chosen elements in SEM are shown in Fig. 7 (b) for convenience.

In "Case-a", simply the domain corresponding to the PML region is considered as free space satisfying the homogenous Helmholtz equation, and the field $u(\vec{r})$ is imposed over both the inner boundary, $\partial\Omega_1$ and the outer boundary, $\partial\Omega_2$. The errors are calculated for the following dimensions: λ=1, r_c=b=0.5, d=c=1, and presented in Table 2 for both Case-a and Case-b. It is worth to point that the errors are larger than the ones presented in Table 1. This is due to the fact that we have deformed elements in this problem.

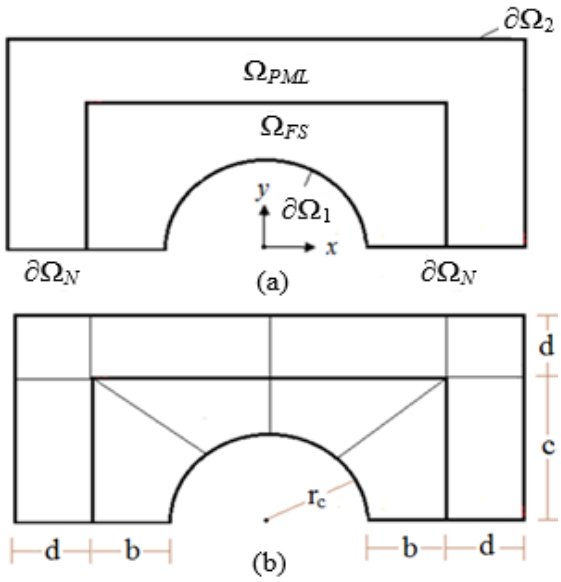

Fig. 7. The problem of the 2D Green's function having a circular inner boundary: (a) the problem definition, and (b) elements in SEM.

Table 2: Maximum relative errors obtained by SEM for the 2D Green's function problem with circular inner boundary

N	α	Err (Case-a)	Err (Case-b)
7	4.40	0.003559	0.001994
8	5.25	0.000382	0.000342
9	6.40	5.24E-05	6.03E-05
10	7.18	6.92E-06	7.77E-06
11	8.41	8.50E-07	9.72E-07
12	9.10	1.06E-07	1.30E-07
13	10.40	1.29E-08	1.50E-08
14	11.16	1.32E-09	1.60E-09
15	12.33	2.44E-10	7.89E-10
16	13.18	6.37E-11	4.65E-10
17	14.22	1.71E-11	3.63E-10
18	15.20	4.62E-12	2.75E-10

B. Scattering cylinder

Next, we have studied scattering by a circular cylinder and considered the following incident plane wave on an infinitely long, circular conducting cylinder of radius r_c (see Fig. 8) of the form $u^i = u_0 e^{-jkx}$.

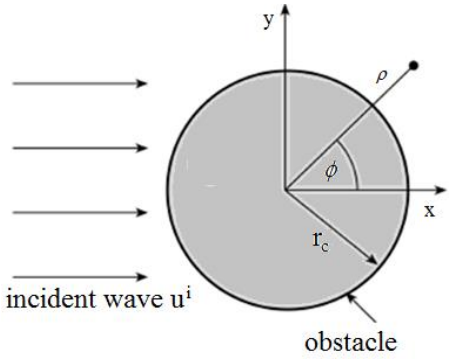

Fig. 8. An incident plane wave to an infinitely-long, circular conducting cylinder.

Because of symmetry in z direction, the problem is a two-dimensional one, and because of symmetry in 2D, only one half of the plane is considered. The scattered field is given analytically in terms of Bessel and Hankel functions as:

$$u^s = -u_0 \sum_{n=-\infty}^{\infty} (-j)^n \frac{J_n(kr_c) H_n^{(2)}(k\rho) e^{jn\phi}}{H_n^{(2)}(kr_c)}. \quad (33)$$

Here, for Case-a, the scattered field given in (33) is imposed on $\partial\Omega_1$ and $\partial\Omega_2$, and for Case-b, the scattered field given in (33) is imposed on $\partial\Omega_1$ only, and zero Dirichlet boundary condition is imposed on $\partial\Omega_2$. Error results are presented in Table 3. As seen from the table, although we have deformed elements, the values of α still give the best accuracy when compared with the accuracy obtained for Case-a. The magnitude of the solution is shown in Fig. 9 at N=10.

Table 3: Maximum relative errors as obtained by SEM for scattering cylinder

N	α	Err (Case-a)	Err (Case-b)
7	4.40	0.010563	0.00305
8	5.25	0.000817	0.00044
9	6.40	7.74E-05	8.02E-05
10	7.18	1.48E-05	1.63E-05
11	8.41	4.46E-06	4.51E-06
12	9.10	1.18E-06	1.18E-06
13	10.40	3.74E-07	3.80E-07
14	11.16	1.24E-07	1.27E-07
15	12.33	3.92E-08	4.78E-08
16	13.18	1.22E-08	3.22E-08
17	14.22	3.78E-09	2.64E-08
18	15.20	1.17E-09	2.21E-08

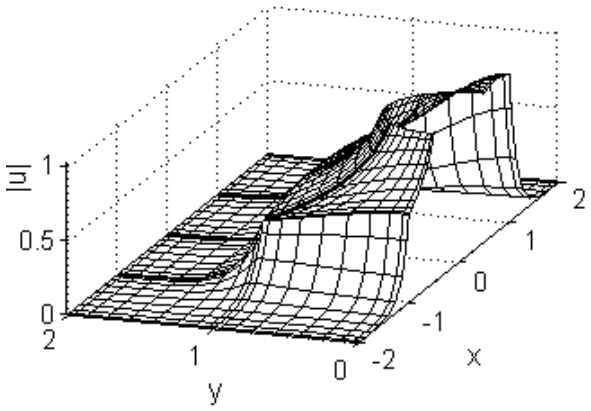

Fig. 9. Magnitude of the scattered field by the cylinder (i.e.: |u|) at N=10.

C. Scattering by large objects

To investigate SEM accuracy using the obtained values of α when scattering by large objects is encountered, we considered a square region 6λ×6λ (standing for the dimensions of the object) whose boundary is $\partial\Omega_1$ (where the field $u(\vec{r})$ is imposed) as shown in Fig. 10. Each of the free space region Ω_{FS}, and the PML region Ω_{PML},

has a width of λ. The computational domain is subdivided into 64 elements so that each element is of λ×λ (λ=1) and has a resolution of N×N. The point source is chosen to be placed in 21 positions as seen from the right side of Fig. 10. Here, we note that because of symmetry, the average relative error of these selected positions is the same as if 121 positions were chosen and distributed uniformly over the object. In each position, the problem (zero Dirichlet bc. is imposed over $\partial\Omega_2$) is solved and the SEM relative error is calculated (i.e.: Case-b). The magnitude of the field when the point source is at position-16 is shown in Fig. 11 at N=7. It should be noted that the maximum incident angle ranges from 45° (for position-1) to 77° (for position-16).

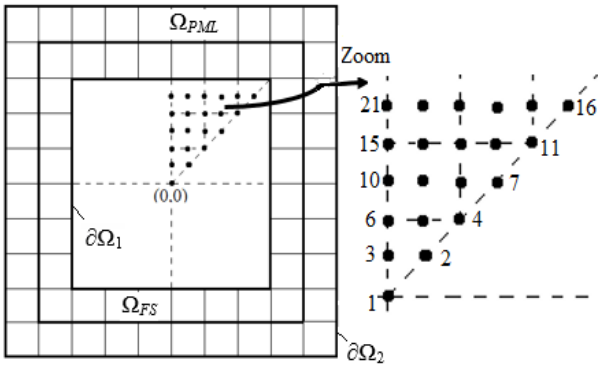

Fig. 10. Scattering by large objects: the computational domain (on the left), selected positions for the point source (on the right).

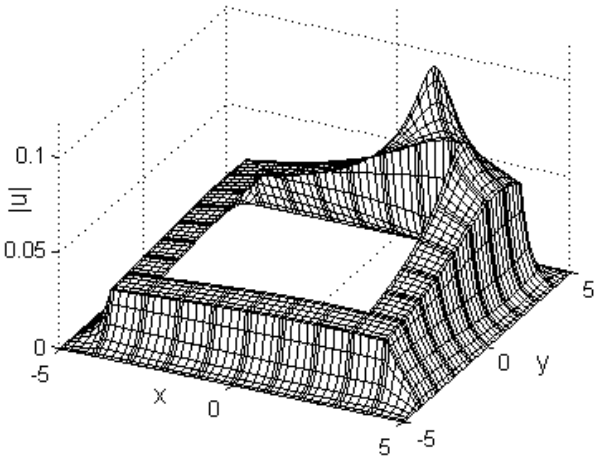

Fig. 11. Plot of |u| for position-16 at N=7.

Although the solutions are obtained by changing the position of the point source whose field is governed by (31), taking the average of the maximum relative errors of all position will give an estimate of the accuracy when a dielectric object is involved. This is due to the fact that the error in our work is normalized with the field, and the solution when a dielectric object exists can be expressed as a linear combination of Hankel function of the second kind of order zero. In Table 4, the average of the errors obtained for the 21 positions are presented.

Table 4: The average of relative errors of the 21 positions

N	α	Average Err
7	4.40	0.006971
8	5.25	0.001451
9	6.40	3.44E-04
10	7.18	1.32E-04
11	8.41	2.91E-05
12	9.10	1.23E-05
13	10.40	2.36E-06
14	11.16	8.71E-07
15	12.33	1.78E-07
16	13.18	7.91E-08
17	14.22	2.68E-08

D. One-dimensional problem

Finally, we considered Helmholtz equation in one dimension over $x \in [-1-\varepsilon, 1+\varepsilon]$, where ε is a real number chosen as 0.001 to avoid singularity (i.e.: to have the solution: $u = \exp(-jkx)$). The domain is divided into two elements each has N points and a length of $1+\varepsilon$. In the first element ($x \in [-1-\varepsilon, 0]$), the homogeneous Helmholtz equation is satisfied and in the second element (PML), the nonhomogeneous Helmholtz equation is satisfied:

$$\frac{1}{a^2}\frac{\partial^2 u}{\partial x^2} + k^2 u = 0, \text{for } x \in [0, 1+\varepsilon]. \quad (34)$$

The boundary conditions are $u(-1-\varepsilon) = \exp(-jk(-1-\varepsilon))$ and $u(1+\varepsilon) = 0$. The maximum relative errors corresponding to the first element are presented in Table 5 for unity wavelength. The imaginary parts of the exact and SEM solution are shown in Fig. 12 at N=18.

Table 5: The maximum relative error of the one-dimensional problem

N	α	Err
7	4.40	0.0065
8	5.25	5.1111e-04
9	6.40	6.0577e-05
10	7.18	6.0067e-06
11	8.41	7.4124e-07
12	9.10	7.1254e-08
13	10.40	8.7009e-09
14	11.16	6.5970e-10
15	12.33	1.0664e-10
16	13.18	8.8274e-12
17	14.22	1.6588e-12
18	15.20	2.3845e-13

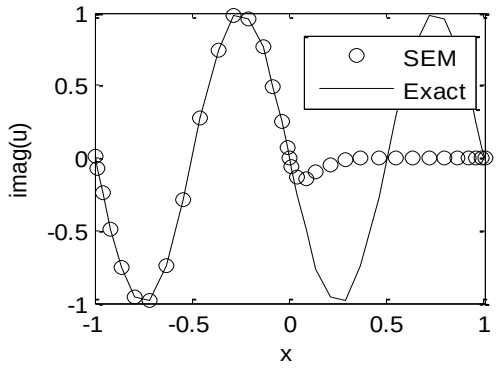

Fig. 12. Imaginary part of the exact and SEM solutions at N=18.

V. CONCLUSION

We have presented in this work the PML formulation for 2D frequency-domain problems and the corresponding SEM formulation taking into account the interface conditions. Based on the numerical results discussed in this paper for different geometries, it is obvious that only one PML layer is required to truncate the computational domain when SEM is used. It is also observed that the provided attenuation factor gives the best accuracy and has almost a linear relationship with the number of points per wavelength ($\text{slope} \approx 0.95$). In addition, the accuracy of scattering by large objects is estimated. Finally, the optimum values of the attenuation factors are used to check the accuracy of SEM for a one-dimensional problem. In conclusion, the applicability of PML in electromagnetic scattering problems by using SEM is very successful in terms of the attenuation factors provided in this work.

ACKNOWLEDGMENT

The first author acknowledges the financial support from Technical Research Council of Turkey (TUBITAK).

REFERENCES

[1] J. P. Berenger, "A perfectly matched layer for the absorption of electromagnetic waves," *Journal of Computational Physics*, vol. 114, pp. 185-200, 1994.

[2] Z. S. Sacks, D. M. Kingsland, R. Lee, and J. F. Lee, "A perfectly matched anisotropic absorber for use as an absorbing boundary condition," *IEEE Transactions on Antennas Propagation*, vol. 43, pp. 1460-1463, 1995.

[3] D. H. Werner and R. Mittra, "New field scaling interpretation of berenger's PML and its comparison to other PML formulations," *Microwave and Optical Technology Letters*, vol. 16, pp. 103-106, 1997.

[4] M. Kuzuoglu and R. Mittra, "A systematic study of perfectly matched absorbers," *Frontiers in Electromagnetics, IEEE Press*, 2000.

[5] J. Lee, T. Xiao, and Q. H. Liu, "A 3-D spectral-element method using mixed-order curl conforming vector basis functions for electromagnetic fields," *IEEE Trans. On Microwave Theory and Techniques*, vol. 54-1, pp. 437-444, January 2006.

[6] J. Lee and Q. H. Liu, "A 3-D spectral-element time-domain method for electromagnetic simulation," *IEEE Trans. On Microwave Theory and Techniques*, vol. 55-5, pp. 983-991, May 2007.

[7] O. Z. Mehdizadeh and M. Paraschivoiu, "Investigation of a two-dimensional spectral element method for helmholtz's equation," *Journal of Computational Phys.*, vol. 189, pp. 111-129, 2003.

[8] S. J. Hesthaven, S. Gottlieb, and D. Gottlieb, "Spectral methods for time-dependent problems," *Cambridge University Press*, 2007.

[9] O. Deville, F. P. Fischer, and E. Mund, "High-order methods for incompressible fluid flow," *Cambridge University Press*, vol. 9, 2002.

[10] J. W. Gordon and A. C. Hall, "Transfinite element methods: blending-function interpolation over arbitrary curved element domains," *Numer. Math*, vol. 21.2, pp. 109-129, 1973.

Ibrahim Mahariq received his B.Sc. degree from the Department of Electrical and Computer Engineering/Palestine Polytechnic University in 2003. He worked there as Teaching Assistant from 2003-2005. He received his M.Sc. degree in Design of Electrical Machines, and his Ph.D. degree in Computational Electromagnetics from Middle East Technical University, Ankara, Turkey. Mahariq was granted TUBITAK scholarship for his Ph.D. studies in 2010, and is currently working in the Department of Electrical and Electronics Engineering at TOBB ETU for research purposes.

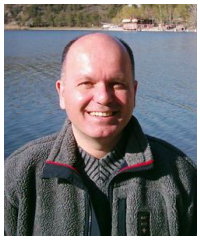

Mustafa Kuzuoglu received his B.Sc., M.Sc., and Ph.D. degrees in Electrical Engineering from Middle East Technical University (METU), Ankara, Turkey, in 1979, 1981, and 1986, respectively. He is currently a Professor with METU. His research interests include computational electromagnetics, inverse problems, and radars.

Hakan I. Tarman received his B.Sc. degree in Mechanical Engineering and Mathematics, and the M.Sc. degree in Mechanical Engineering from Boğaziçi University, İstanbul, Turkey. He received his Ph.D. degree in Applied Mathematics from Brown University, Providence, Rhode Island, USA. He is currently a Professor with the Department of Engineering Sciences, Middle East Technical University, Ankara, Turkey.